Superhydrophobic-Superhydrophilic Binary Micropatterns by Localized Thermal Treatment of Polyhedral Oligomeric Silsesquioxane (POSS)-Silica Films

Thomas M. Schutzius,[a] Ilker S. Bayer,[b] Gregory M. Jursich,[a] Arindam Das,[a] and

Constantine M. Megaridis[a],*

[a] Department of Mechanical and Industrial Engineering University of Illinois at Chicago, Chicago, IL 60607, USA

[b] Center for Biomolecular Nanotechnologies @UNILE, Istituto Italiano di Tecnologia Via Barsanti, 73010 Arnesano (LE), Italy

*Corresponding Author:

Email: cmm@uic.edu, phone: +1 312 996-3436, Fax: +1 312 413 0447

Surfaces patterned with alternating (binary) superhydrophobic-superhydrophilic regions can be found naturally, offering a bio-inspired template for efficient fluid collection and management technologies. We describe a simple wet-processing, thermal treatment method to produce such patterns, starting with inherently superhydrophobic polysilsesquioxane-silica composite coatings prepared by spray casting nanoparticle dispersions. Such coatings become superhydrophilic after localized thermal treatment by means of laser irradiation or open-air flame exposure. When laser processed, the films are patternable down to micrometer scales (~100 μm). The dispersions consist of hydrophobic fumed silica (HFS) and methylsilsesquioxane resin, which are dispersed in isopropanol and deposited onto various substrates (glass, quartz, aluminum, copper, stainless steel). The coatings are characterized by advancing, receding, and sessile contact angle measurements before and after thermal treatment to delineate the effects of HFS filler concentration and thermal treatment on coating

wettability. SEM, XPS and TGA measurements reveal the effects of thermal treatment on surface chemistry and texture. The thermally-induced wettability shift from superhydrophobic to superhydrophilic is interpreted with the Cassie-Baxter wetting theory. Several micropatterned wettability surfaces demonstrate potential in pool boiling heat transfer enhancement, capillarity-driven liquid transport in open surface-tension-confined channels (e.g., lab-on-a-chip), and select surface coating applications relying on wettability gradients. Advantages of the present approach include the inherent stability and inertness of the organosilane-based coatings, which can be applied on many types of surfaces (glass, metals, etc.) with ease. The present method is also scalable to large areas, thus being attractive for industrial coating applications.

1. Introduction

Polyhedral Oligomeric Silsesquioxanes or, in short polysilsesquioxanes (POSS), are organic–inorganic hybrid materials having unique molecular structures.[1] POSS resins are a class of silicon compounds with the empirical formula $RSiO_{1.5}$, where R denotes hydrogen or an alkyl, alkylene, aryl, or arylene group. The POSS name is derived from one and one half (1.5) or sesquistoichiometry of oxygen bound to silicon. POSS molecular building blocks can be tuned for desired optical, structural and mechanical properties.[2] The most common form of POSS is a three dimensional Si-O cage framework, commonly known as a POSS nanocage. Among POSS compounds, solution-processable hydrogen silsesquioxane (HSQ) or methylsilsesquioxane (MSQ) resins generally find applications as low-dielectric materials for integrated circuit devices[3-8] and are also used as an alternative route to produce silica coatings.[9, 10] For high temperature applications, POSS resins may have greater advantages over their organic polymer counterparts due to their inherently higher bond strength.[11, 12] Silsesquioxanes can be produced with a variety of pendant chemical groups (i.e., alkyl, aryl, etc.), thus allowing appreciable solubility in organic solvents for solution processing; MSQ is

2

expected to be hydrophobic due to the presence of methyl groups. Further enhancement of film hydrophobicity may be attained by introducing hydrophobic inorganic nanoparticles, such as hydrophobic fumed silica (i.e., silica modified by silanes or siloxanes), into the MSQ film. These filler particles not only lower the surface energy of the films, but also affect surface texture, two factors known to significantly influence hydrophobicity.[13, 14] With proper combination of hydrophobic nanoparticles, it seems possible to achieve superhydrophobic coatings based upon POSS materials, thereby circumventing problems associated with organic polymers, and in turn, offering improved coating thermal stability and scratch resistance. Finally, due to the ability of POSS to oxidize[10] and generate hydrophilic functional groups (i.e., silanol),[9] it may be possible to induce spatially abrupt wettability transitions in such coatings (from superhydrophobic to superhydrophilic) if, for example, hydrophobic Si-CH$_3$ bonds of MSQ were to be replaced with hydrophilic functional groups in select locations. Similar logic applies for silane or siloxane modified silica (e.g., HFS) as under oxidizing conditions silicon will readily abandon linkages with hydrogen or carbon in preference for oxygen, thus inducing hydrophilicity.[11] If it is possible to induce a wettability transition to a POSS nanocomposite coating by a fast thermally assisted process—such as with flame exposure or laser irradiation—then one may be able to fabricate chemically stable surfaces patterned with superhydrophobic and superhydrophilic area regions by large-area processing. With laser-beam heating, patterning the wettability at the micrometer scale may be possible.

The advantages of alternating hydrophobic-hydrophilic areas have been extolled in a recent patent,[15] where a sol-gel method was used to apply transparent superhydrophobic silica coatings whose wettability could be locally modified continuously from superhydrophobic to superhydrophilic by masked UV exposure. In the open literature, alternating superhydrophobic-superhydrophilic area patterns with well-defined repeatable features have been reported only by a handful of groups. For example, Zhai et al.[16] generated hydrophilic

patterns on superhydrophobic surfaces by selective deposition of polyelectrolyte/water/2-propanol mixtures; such surfaces mimic the water harvesting behavior of the Stenocara beetle's back.[17] Garrod et al.[18] utilized a two-step, plasma chemical approach to generate said surfaces; their applications include fog harvesting, microfluidics, and biomolecule immobilization. Other reported patterning approaches include photo degradation of hydrophobic chemistry,[19, 20] and photo-induced modification of hydrophobic/hydrophilic chemistry.[21] In addition, highly desirable surface-tension-confined (STC) micro channels in two[22] and three dimensions[23] can also be realized through wettability patterning techniques. UV-irradiation has been used[24] to generate such micropatterns. Most recently, Zahner et al.[25] used UV-initiated photo grafting to generate virtual microfluidic channels in the form of superhydrophilic micropatterns on a superhydrophobic porous polymer film; one possible application is two-dimensional peptide separation.[26] However, most of these patterning techniques require the use of masks (e.g., plasma chemical,[18] photo degradation techniques,[19, 20] photo-induced technique,[21] UV-irradiation[24, 25]) or closed chambers.[18] Masks limit the flexibility in changing the type of pattern on-the-fly, while chambers limit scalability and increase the patterning costs. Finally, in some superhydrophilic patterning techniques, the property is not permanent, as is the case with UV-irradiation of TiO_2 containing coatings.[24] Such coatings also require large concentrations of filler particles to attain superhydrophilicity,[24] which may reduce their adhesion and durability as compared with other coating systems. None of the previous works on superhydrophobic-superhydrophilic area patterning involved silsesquioxanes.

We report herein spray-based fabrication of large-area superhydrophobic MSQ-HFS nanocomposite coatings, which are capable of becoming superhydrophilic when thermally treated by simple flame or laser exposure. Micro-patterned wettability—with alternating areas of superhydrophobicity and superhydrophilicity—is demonstrated for the first time using

localized thermal treatment applied by computer controlled CO_2 (infrared) laser irradiation in open air. Open STC micro-channels are thus formed by large-area, two-step processing (i.e., spray and laser treatment). Spray deposition and CO_2 laser processing (thermal treatment) are two efficient industrial processes, making them ideally suited for large-area applications. It takes seconds of laser treatment to form a 0.1 m long open STC micro-channel. Applications are envisioned in microfluidics and other small liquid volume handling technologies. Due to their ability to withstand temperatures well above the boiling point of water, one possible application of such patterned binary-wettability coatings is in the area of enhanced heat transfer (e.g., pool boiling). The present technique is not substrate limited, therefore such patterns can be applied on thermally-conductive materials (e.g., metals), which are necessary in heat transfer applications at elevated temperatures. This feature, along with the thermal stability of the present patterns, opens new horizons in technologies involving high temperature fluids.

2. Results and Discussion

The purpose of introducing hydrophobic, inorganic nanoparticles into the spray dispersion is to affect the coating surface texture resulting after application and drying—a well-established approach for achieving superhydrophobicity.[13, 14, 27] **Figure 1a** illustrates the characteristic micro-cluster surface morphology of a MSQ-HFS coating (1.0 HFS/MSQ mass ratio) applied by spray, while the higher magnification image in Fig. 1b displays the resulting nanotexture due to HFS particles embedded in the MSQ matrix. Such hierarchical surface texture is known to produce superhydrophobicity on both artificial and natural surfaces. **Figure 2a** presents the advancing (θ_{adv}^*) and receding (θ_{rec}^*) contact angles as functions of HFS concentration in the MSQ matrix. The two curves display trends similar to those seen in the classic experiments of Johnson and Dettre[28] where advancing and receding contact angles were quantified with respect to increasing substrate roughness. Contact angle hysteresis

$(\theta^*_{adv} - \theta^*_{rec})$ initially increases with HFS filler content (i.e. surface roughness), followed by an abrupt decrease as the HFS concentration increases further, indicating a wetting state transition (i.e., Wenzel to Cassie-Baxter).[29, 30] Beyond a 1.0 HFS/MSQ mass ratio, the coating becomes superhydrophobic (i.e. $\theta^*_{adv} > 150°$). The Cassie-Baxter (non-wetting) state should be realized if the true (Young's) contact angle (θ) satisfies the condition

$$\theta > \theta_c, \text{ with } \cos\theta_c = -\frac{1-\Phi_s}{r-\Phi_s} \tag{1}$$

where the surface roughness factor r is defined as the ratio of true rough area to its projected value, Φ_s represents the fractional solid surface area in contact with the liquid ($\Phi_s < 1$), and θ_c is the critical contact angle.[31] For very rough surfaces with a high concentration of filler particles or rough surface texture due to the spray process itself, it follows that $r \gg \Phi_s$, and the cosine of the critical angle, θ_c, is proportional to $-r^{-1}$; thus, for highly rough, hydrophobic surfaces ($\theta > 90°$), the value of θ_c from **Eq. 1** decreases, and Cassie-Baxter becomes the most probable wetting state, not considering metastable wetting states. As shown in Fig. 2a, the contact angle hysteresis is 8° at a HFS/MSQ mass ratio of 1.5, which designates a self-cleaning surface (droplets roll off the surface under only a slight substrate tilt). Further rise in hydrophobic filler concentration results in a further decrease of contact angle hysteresis. Figure 2b presents sessile contact angle values (θ^*) for the previously characterized coatings, before and after flame treatment. For all cases where HFS filler is incorporated into MSQ, the coatings achieve a zero-valued or immeasurably small apparent contact angle after flame treatment, thus indicating superhydrophilicity. Refer to **Fig. S1** in Supporting Information for a sequence of images demonstrating flame treatment and the subsequent superhydrophilic property. The dramatic transition from non-wetting to fully-

wetting state should be observed if the cosine of the true (Young's) contact angle satisfies the condition

$$\theta < \theta_C \text{ with } \cos\theta_C = \frac{1-\Phi_S}{r-\Phi_S} \tag{2}$$

where θ_C ($0° < \theta_C < 90°$) is the critical contact angle for transition to wetting. If the condition for θ in **Eq. 2** is satisfied, then the liquid penetrates the surface texture but partial wetting remains due to islands emerging above the absorbed film (i.e., $\theta \neq 0°$).[31] Regarding morphological changes as a result of brief flame treatment, the coating is not observed to undergo drastic changes, i.e., r remains relatively high. In the limit of $\Phi_S << r$, Eq. 2 becomes

$$\theta < \theta_C \text{ with } \cos\theta_C \approx \frac{1}{r} \quad . \tag{3}$$

Therefore, for highly rough, hydrophilic surfaces ($\theta < 90°$), the value of θ_C from Eq. 2 is high, and the superhydrophilic state becomes most probable—alternatively stated, highly wettable surfaces require less roughness to display superhydrophilicity.

To delineate the effects of HFS filler content (which affects texture) and thermal treatment (which affects surface energy), **Fig. 3** presents apparent advancing contact angles for spray cast MSQ-HFS composite films vs. θ_{adv} of spin-coated MSQ before and after flame treatment. The values of θ_{adv} for spin-coated MSQ before and after flame treatment were measured to be 95° and 23°, respectively. Two HFS/MSQ mass ratios (0.25 and 1.5) are represented in Fig. 3. Also plotted in the same figure are the lines for two theoretical cases, namely Cassie-Baxter (**Eq. 4** below with $\Phi_s = 0.04$) and Wenzel (**Eq. 5** below with $r = 1.48$). For the Cassie-Baxter case, the apparent contact angle is given by

$$\cos \theta^* = -1 + \Phi_s (\cos \theta + 1) \qquad (4)$$

while for the Wenzel case

$$\cos \theta^* = r \cos \theta \qquad (5)$$

As stated previously, for the heat-treated (wettable) MSQ, $\theta_{adv} = 23°$. Taking θ_{adv} as a conservative approximation of θ_C, and substituting into **Eq. 3**, we see that the lower threshold value of r for the validity of Eq. 3 comes as, $r^* = 1/\cos\theta_{adv} \approx 1.1$, which is an easily attainable roughness ratio. It is possible to quantify the roughness ratio of the coating prior to flame treatment by utilizing Eq. 5; the only requirement is that the liquid droplet be in a Wenzel wetting state. At 0.25 HFS/MSQ mass ratio, the measured θ_{adv}^* value is relatively small (~97°; see Fig. 2a) and the hysteresis is high (~30°; Fig. 2a), which are characteristic traits of droplets in a partially wetting Wenzel state, thus allowing use of Eq. 5 to quantify r (note that this particular point falls in the hydrophobic regime of Fig. 3 and is prior to coating flame treatment). The dashed line Wenzel fit with $r = 1.48$ shows that the 0.25 HFS/MSQ mass ratio coating is consistent with a roughness value sufficiently higher than the threshold value of 1.1, thus allowing the most stable wetting state, *after flame treatment*, to be superhydrophilic (assuming negligible morphological changes due to flame treatment). [†] Intuitively this corresponds to a MSQ-HFS film that is sufficiently wettable (i.e., possesses high surface energy) to require only a low level of roughness for superhydrophilicity to be energetically favored. Also in Fig. 3, the data point for untreated 1.5 HFS/MSQ mass ratio coating resides in the lower left quadrant, suggesting that the water droplet is in a stable Cassie-Baxter wetting state, and not a metastable one (metastable states generally reside in the lower right

---

[†] While local gas temperatures in propane flames can rise to 2200 K, small propane flames impinging onto coated bulk surfaces for 1–2 seconds are not capable of raising coating temperatures up to the melting point of silica (~1900 K). Consequently, during flame treatment, the coating temperatures stay well below this critical value, thus eliminating the possibility of significant morphological changes in the coating texture. See Fig. S6 in ESI for SEM images of a flame-treated MSQ-HFS coating.

quadrant of Fig. 3). Thus, this point can be fitted with the Cassie-Baxter curve, $\Phi_s = 0.04$, suggesting a very low fraction of the textured solid being in contact with the beaded liquid.

CO_2 lasers offer a controlled approach to thermal treatment due to their ability to deliver high levels of energy to localized surface areas. Since most materials are opaque at 10 μm (laser wavelength), CO_2 lasers offer a robust approach to surface heat treatment. Heating can be regulated by tuning beam size and energy, as well as beam exposure. **Figure 4** quantifies the effect of laser treatment on wettability of pure MSQ and MSQ-HFS films as a function of laser exposure. For these tests, laser power was held constant at ~1 W and the laser translation speed was varied. For sufficiently high fluence (i.e., >150 J cm^{-2}), the films underwent a wettability transition to complete wetting, as indicated by the very low values of θ^* in Fig. 4, and as previously observed for the flame-treated films (cf. Fig. 2b). It is instructive to compare the temperature ranges attained in both thermal treatment processes. In the case of propane flames, the flame temperature is ~2,200 K. For laser treatment, direct temperature measurement is difficult due to the low exposure time to the laser beam. For a laser spot diameter (d_s) of ~25 μm and a translation speed (v) of 2.0 cm s^{-1} (the speed used for all subsequent laser treatments), the exposure time scales like $d_s/v \approx 1$ ms. The corresponding rise in surface temperature (ΔT) can be estimated using an expression applicable for a semi-infinite solid medium heated on a spot (see Eq. S1 in Supporting Information).[32, 33] After only $t = 0.022$ ms, ΔT ~2,000 K, a temperature that is comparable with the propane flame temperature. So while this temperature is sufficient to explain wettability transition as a result of laser treatment, it is insufficient to explain morphological changes. At $t = 0.025$ ms, ΔT becomes 2,230 K which is sufficient to cause silica boiling. Significant removal of coating material should be expected as thermal treatment extends far further than the time required to reach temperatures required for wetting transitions, potentially resulting in channel formation

(for a single laser pass) or a thinner coating (for total surface treatment), the latter being advantageous for heat transfer applications, where the thermal resistance associated with thicker coating treatments must be minimized.

It is important to establish the minimum spatial feature size during CO_2 laser processing. The diameter of the focused laser spot is defined as

$$d_s = \frac{4}{\pi} \lambda \frac{f}{D} \qquad (6)$$

where f is the beam focal length, D the initial beam diameter, and λ the beam wavelength.[34] We employed a high power density lens with a 25 μm spot diameter. According to the manufacturer, it is feasible to produce a finer spot diameter by diverging the beam, but this generally resulted in inadequate thermal treatment, i.e., the treated surfaces did not become superhydrophilic. Optimization of the laser-lens-to-substrate distance was done by observing when superhydrophilicity was or was not achieved (see **Fig. S2** in Supporting Information). It is also important to understand the wetting transition between hydrophobic and hydrophilic areas, and more importantly, the spatial extent of this transition. A sharp transition will allow the surface to confine liquids, which has important ramifications on microfluidics and lab-on-a-chip applications.

Figure 5a presents a CO_2 laser patterned hydrophilic circular spot in a hydrophobic background. Fig. 5b-d presents a hydrophilic spot being characterized by an advancing water contact angle measurement; the edges of the hydrophilic spot are marked by dark arrows. As the water is dispensed from the needle, the droplet readily advances to the edge of the hydrophilic pattern, and once there, it pins. The droplet remains pinned at that location as it grows above it, until it achieves a high contact angle value, and begins to advance once again, but this time with a high contact angle, indicating superhydrophobicity. This experiment

demonstrates the spatially abrupt wettability transition on the patterned surface. SEM analysis also confirms a sharp transition of the coating from superhydrophobic to superhydrophilic, as shown in Fig. 5e, left-to-right through the dashed-line boundary. **Figure 6a-d** shows examples of STC microchannels with and without deposited water; **e-f** show SEM micrographs of the channels with increasing magnification. It is obvious that laser-treatment ($I \approx 0.2\,\text{MW cm}^{-2}$, $d_s = 25\,\mu\text{m}$, $v = 2.0\,\text{cm s}^{-1}$) has removed much of the coating material, thus creating a physical channel. Figure 6g shows a high-magnification micrograph of the patterned area where laser treatment caused cellular morphology. While during flame treatment the pre-existing surface roughness remained relatively unchanged (as confirmed from SEM analysis; see Fig. S6 in Supporting Information), the laser treatment actually produced its own unique surface texture, facilitating superhydrophilicity. Figure 6f actually shows coating areas that have been completely stripped by the laser processing; these areas form apparently bare islands with the remaining coated sections percolating, thus allowing superhydrophilicity to persist. Further optimization of spray processing (i.e., increased coating thickness) should reduce the likelihood of bare-island formation. An important property of STC channels is the average flow velocity of water in them. In the case of a 7.2 mm-long 0.18 mm-wide channel formed with the present procedure, the average water flow velocity was 2.5 mm s^{-1}, which is comparable to speeds attained by others in similar sized channels.[25]

Laser-treated areas appear visually different than non-treated areas. As shown before (Fig. 6), laser processing removes the top portion of the coating. The resulting surface is a thin, glassy coating devoid of the micro-features originating from spray application and appears more optically transparent (see **Figure S3** in Supporting Information). For heat transfer applications, a thin coating or surface treatment is desirable, as minimal thermal resistance is required. For pool boiling applications, it has been recently reported that selective patterned areas of hydrophobicity and hydrophilicity on surfaces, improves heat transfer characteristics (i.e.,

heat transfer coefficient, critical heat flux).[35] The demonstrated feature sizes were in the ~100 μm range with either hydrophobic or hydrophilic networks. **Figure 7a-b** show laser patterning of similar ~100 μm repeatable feature sizes of either hydrophobic or hydrophilic nature, while **c** shows what happens when the patterned surface shown in Fig. 7b is subjected to nucleate boiling conditions; the hydrophobic islands act as preferred nucleation sites for boiling, in line with previously reported results.[35] An important property of these MSQ-HFS films is their ability to maintain extreme wetting properties during and after heating. Determination of the temperature at which these surfaces change wettability is important. **Figure 8** presents water droplet sliding angle measurements as a function of temperature treatment of the coating on a hot plate for one hour. At treatment temperatures below 300°C, the sliding angles are well below 10°, indicating self-cleaning ability for these coatings. For treatment above 300°C, the coating begins to undergo a change in its superhydrophobic property. After treatment at 500°C, the coating ceases to display droplet sliding behavior with the water droplets remaining pinned, indicating a full-loss of superhydrophobicity and the Cassie-Baxter wetting state, and marking a *temperature limit* for the application of this coating. The ability to maintain superhydrophobic behavior even after thermal treatment at 300°C (i.e., no degradation, no melting, etc.) puts this composite coating in class with some of the high-performance thermoplastics which have melting points above 300°C (e.g., poly(ether ether ketone)).

In order to further explore the thermal properties of the MSQ and HFS coating ingredients, **Fig. 9** presents two separate TGA plots, one for HFS **a** and the other for pure MSQ **b**. In the case of HFS tested under nitrogen atmosphere conditions, no significant mass loss was detected, while under oxidative conditions of artificial air (80% N_2 , 20% O_2), a 2.3 wt.% mass loss was detected between 530-630°C. It is suggested that this mass loss is attributed to oxidation of alkyl groups in the HFS, which results in formation of –OH containing function

groups and evolution of volatile CO, CO_2 and H_2O. According to the manufacturer, the concentration of carbon in the HFS, as induced by the wettability modification of silica, is in the range of 0.7-1.3 wt.%. This is quite close to the TGA mass loss (2.6 wt.%) seen in the oxidizing atmosphere, and thus carbon presence in the HFS could be responsible for this mass reduction. HFS becomes dispersible in water after thermal treatment at 900°C in artificial air (see inset image in Fig. 9a, vial 3) and retains its white color (i.e., no pyrolysis), supporting alkyl group oxidation as the probable mass loss mechanism. For MSQ in Fig. 9b, the TGA shows three significant mass losses at 159°C, 377°C, and 719°C for oxidizing conditions (artificial air) and at 154°C, 406°C, and 771°C for inert conditions (nitrogen). Regarding the first mass loss (159°C), the coating remains self-cleaning after thermal treatment at 200°C (see Fig. 8), so this mass loss is irrelevant in the context of superhydrophobicity. A previous study attributed such mass loss to condensation of silanol groups and loss of siloxane.[36] For the mass loss of MSQ at medium temperature (300-500°C), this is the temperature range where loss of superhydrophobicity is observed. The effect of mass loss on wettability at ~400°C is unclear, but the associated loss of superhydrophobicity there may be due to MSQ melting, which affects surface texture—a major factor in superhydrophobicity—more than it is due to chemical changes and mass loss of MSQ. At 500°C, the coating begins to undergo a color change from its original white to black, and chemical changes begin to play a prominent role. Heating MSQ in air or O_2 above 600°C results primarily in the formation of SiO_2, which is used for production of silica glasses.[9] In the case of flame or laser treatment in open air, one can expect more extreme thermal treatment than that delivered by TGA testing; transformation of hydrophobic methyl groups to hydrophilic –OH groups can thus be expected.

High-resolution XPS analysis of silicon, oxygen, and carbon was done on untreated, flame treated, and laser treated MSQ-HFS (1.0 HFS/MSQ mass ratio) coatings. This analysis

supported the TGA data, in turn, suggesting increased concentration of Si-O bonding and reduced concentration of Si-R bonding (i.e., methyl) with heating, both consistent with the observed increased silica concentration and decreased hydrophobicity (**Fig. S4** in Supporting Information).

3. Conclusion

Thermally-stable (at temperatures below 400°C) polysilsesquioxane-silica superhydrophobic nanocomposite coatings have been demonstrated by spray casting nanoparticle dispersions in alcohol. The coatings, after drying, are intrinsically superhydrophobic, but are capable of becoming superhydrophilic by either flame or CO_2 laser treatment in open air. The latter allows imprinting of superhydrophilic patterns onto the coatings with feature size around ~100 μm. The interface between heat-treated and untreated regions was sharp, as determined by advancing CA and SEM analysis. Chemical analysis suggests that the wettability transition is due to oxidation of hydrophobic methyl groups. Wettability transitions were interpreted within the Wenzel and Cassie-Baxter wetting theories. Simple water pool boiling experiments showed the promise of such patterned surfaces for enhanced heat transfer applications. Water velocities of ~2 mm s^{-1} in true micro channels offers promise for fabricating surface tension confined micro-channels (STC). Advantages of the present approach include inherent thermal stability over organic-based coatings, as well as scalability to large-area applications.

4. Experimental

Materials: The materials used were: isopropanol (IPA, Sigma-Aldrich, USA), methylsilsesquioxane resin (Gelest, Inc.; 19-21 wt.% in a mixture of methanol, n-butanol, and isopropanol), and hydrophobic fumed silica, Aerosil®; silane or siloxane modified silica).

Dispersion and Coating Preparation: In a 20 mL glass vial, hydrophobic fumed silica and IPA were combined and sonicated (Sonics®, 750 W, High Intensity Ultrasonic Processor, 13 mm diameter tip at 30 % amplitude) to form a suspension. Once a stable HFS-IPA suspension was formed, the MSQ solution in alcohol was added, and the entire dispersion was sonicated until a stable dispersion formed. Typical sonication procedures lasted 1-2 min under ambient conditions; longer sonication times resulted in undesirable boiling loss of the alcohol solvents. Stable dispersions (Table 1) were then spray cast with an airbrush atomizer (Paasche VLS, siphon feed, 0.73 mm nozzle) onto stainless steel, aluminum foil, copper, quartz, and glass slide substrates at a spray distance of 10 cm and were subsequently heated with a heat gun (Proheat® Varitemp® PH-1200, 1300 W max) to immediately remove solvents, and an oven at 130ºC for 1 hr to allow the coating to dry. Alternatively, thermal treatment—for the purposes of inducing a wettability transition—was done with either a propane flame or a CO_2 laser (100 W max, 25 μm spot size, mounted on a computer-controlled 3-axis stage; output power is controlled by a percentage of maximum power, i.e., 1.0% power corresponds to ~1 W). For some samples, laser patterning was used to form repeating islands of either hydrophobic or hydrophilic nature.

Characterization: Environmental scanning electron microscope (ESEM, Philips XL30 ESEM-FEG) and scanning electron microscope (SEM, Hitachi S-3000N, variable pressure) images were obtained after samples were sputter-coated with a conformal 5 nm thick layer of Au-Pd or Pt-Pd. X-ray photoelectron spectroscopy (XPS, Kratos AXIS-165) was performed on heat gun-treated, flame-treated, and laser-treated MSQ-HFS coatings deposited on stainless steel, to investigate the effect of thermal treatment on the surface chemistry of the coating. Thermogravimetric analysis (TGA) was performed to determine degradation temperatures and reveal the related mechanisms. Sessile, advancing and receding contact angle values were obtained with a backlit, optical, high speed image acquisition setup

(Redlake MotionPro) utilizing 10 μL water droplets. Coating heat treatment—for the purposes of analyzing the effect of temperature on wettability—was done with a standard hot-plate. Each sample was kept at a constant, elevated temperature for 1 hr (e.g., 200°C, 300°C, etc.) and then was removed and allowed to cool down to ambient temperature. Each sample was subsequently characterized by sliding angle measurements with 5.0 μL water droplets on a tilting stage with 1° accuracy.

1. G. Z. Li, L. C. Wang, H. L. Ni and C. U. Pittman, *Journal of Inorganic and Organometallic Polymers*, 2001, **11**, 123-154.
2. H. W. Ro and C. L. Soles, *Materials Today*, 2011, **14**, 20-33.
3. M. G. Albrecht and C. Blanchette, *Journal of the Electrochemical Society*, 1998, **145**, 4019-4025.
4. M. J. Loboda, C. M. Grove and R. F. Schneider, *Journal of the Electrochemical Society*, 1998, **145**, 2861-2866.
5. Y. K. Siew, G. Sarkar, X. Hu, J. Hui, A. See and C. T. Chua, *Journal of the Electrochemical Society*, 2000, **147**, 335-339.
6. C. Y. Wang, Z. X. Shen and J. Z. Zheng, *Applied Spectroscopy*, 2000, **54**, 209-213.
7. L. H. Lee, W. C. Chen and W. C. Liu, *Journal of Polymer Science Part A-polymer Chemistry*, 2002, **40**, 1560-1571.
8. C. C. Yang and W. C. Chen, *Journal of Materials Chemistry*, 2002, **12**, 1138-1141.
9. R. M. Laine, J. A. Rahn, K. A. Youngdahl, F. Babonneau, M. L. Hoppe, Z. F. Zhang and J. F. Harrod, *Chemistry of Materials*, 1990, **2**, 464-472.
10. R. H. Baney, M. Itoh, A. Sakakibara and T. Suzuki, *Chemical Reviews*, 1995, **95**, 1409-1430.
11. E. G. Rochow, *An Introduction to the Chemistry of the Silicones*, John Wiley & Sons, 1946.
12. W. J. Zhou, H. Yang, X. Z. Guo and J. J. Lu, *Polymer Degradation and Stability*, 2006, **91**, 1471-1475.
13. I. S. Bayer, M. K. Tiwari and C. M. Megaridis, *Applied Physics Letters*, 2008, **93**, 173902.

14.   M. K. Tiwari, I. S. Bayer, G. M. Jursich, T. M. Schutzius and C. M. Megaridis, *ACS Applied Materials & Interfaces*, 2010, **2**, 1114-1119.
15.   *US Pat.,* 7,485,343, 2009.
16.   L. Zhai, M. C. Berg, F. C. Cebeci, Y. Kim, J. M. Milwid, M. F. Rubner and R. E. Cohen, *Nano Letters*, 2006, **6**, 1213-1217.
17.   A. R. Parker and C. R. Lawrence, *Nature*, 2001, **414**, 33-34.
18.   R. P. Garrod, L. G. Harris, W. C. E. Schofield, J. McGettrick, L. J. Ward, D. O. H. Teare and J. P. S. Badyal, *Langmuir*, 2007, **23**, 689-693.
19.   V. Jokinen, L. Sainiemi and S. Franssila, *Advanced Materials*, 2008, **20**, 3453-3456.
20.   K. Tadanaga, J. Morinaga, A. Matsuda and T. Minami, *Chemistry of Materials*, 2000, **12**, 590-592.
21.   S. J. Pastine, D. Okawa, B. Kessler, M. Rolandi, M. Llorente, A. Zettl and J. M. J. Frechet, *Journal of the American Chemical Society*, 2008, **130**, 4238-4239.
22.   P. Lam, K. J. Wynne and G. E. Wnek, *Langmuir*, 2002, **18**, 948-951.
23.   J. T. Lee, M. C. George, J. S. Moore and P. V. Braun, *Journal of the American Chemical Society*, 2009, **131**, 11294-11295.
24.   X. Zhang, H. Kono, Z. Liu, S. Nishimoto, D. A. Tryk, T. Murakami, H. Sakai, M. Abe and A. Fujishima, *Chemical Communications*, 2007, 4949-4951.
25.   D. Zahner, J. Abagat, F. Svec, J. M. J. Frechet and P. A. Levkin, *Advanced Materials*, 2011, **23**, 3030-3034.
26.   Y. H. Han, P. Levkin, I. Abarientos, H. W. Liu, F. Svec and J. M. J. Frechet, *Analytical Chemistry*, 2010, **82**, 2520-2528.
27.   P. N. Manoudis, I. Karapanagiotis, A. Tsakalof, I. Zuburtikudis and C. Panayiotou, *Langmuir*, 2008, **24**, 11225-11232.
28.   R. E. Johnson and R. H. Dettre, in *Contact Angle, Wettability, and Adhesion*, American Chemical Society, 1964, vol. 43, ch. 7, pp. 112-135.
29.   R. N. Wenzel, *Industrial & Engineering Chemistry*, 1936, **28**, 988-994.
30.   A. B. D. Cassie and S. Baxter, *Transactions of the Faraday Society*, 1944, **40**, 546-551.
31.   P. G. de Gennes, F. Brochard-Wyart and D. Quere, *Capillarity and Wetting Phenomena: Drops, Bubbles, Pearls, Waves*, Springer Verlag, 2004.
32.   M. von Allmen, *Laser-Beam Interactions with Materials*, Spinger-Verlag, Berlin, 1987.
33.   G. Allcock, P. E. Dyer, G. Elliner and H. V. Snelling, *Journal of Applied Physics*, 1995, **78**, 7295-7303.
34.   Z. Illyefalvi-Vitez, *Microelectronics Reliability*, 2001, **41**, 563-570.
35.   A. R. Betz, J. Xu, H. H. Qiu and D. Attinger, *Applied Physics Letters*, 2010, **97**, 141909.
36.   F. I. Hurwitz, P. Heimann, S. C. Farmer and D. M. Hembree, *Journal of Materials Science*, 1993, **28**, 6622-6630.
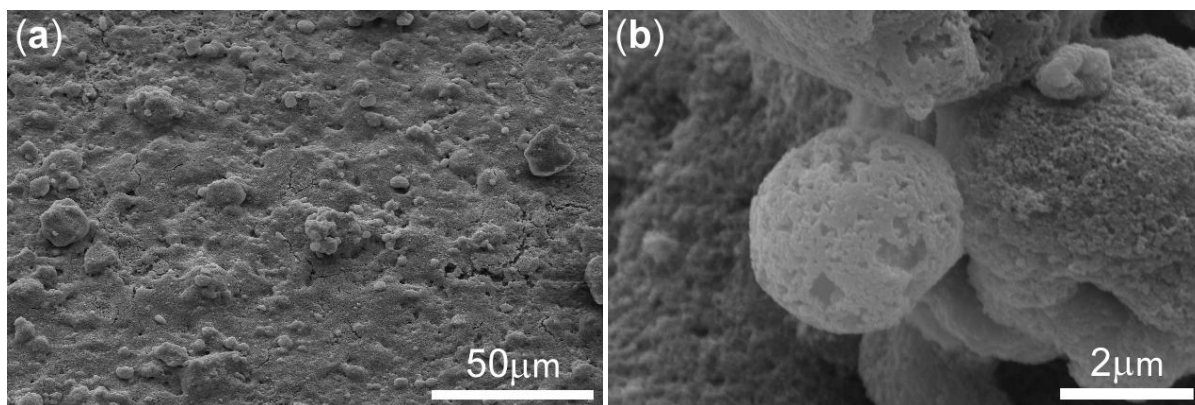
Figure 1. ESEM images of superhydrophobic MSQ-HFS coating (1.0 HFS/MSQ mass ratio) with increasing magnification from (a) to (b).
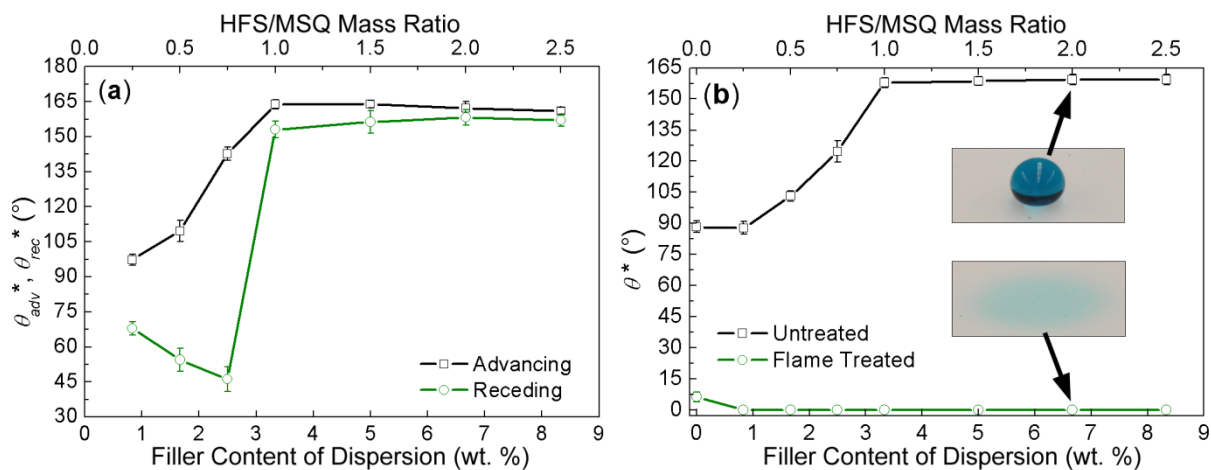
Figure 2. (a) Apparent advancing (θ^*_{adv}) and receding (θ^*_{rec}) contact angles, and (b) sessile θ^* contact angle vs. filler content of the dispersion (bottom axis) and HFS/MSQ mass ratio (top axis). Insets in (b) show blue-dyed water droplets: Top demonstrating beading on the untreated superhydrophobic surface; bottom demonstrating superhydrophilicity (fully spread droplet) attained after the coating was flame-treated.
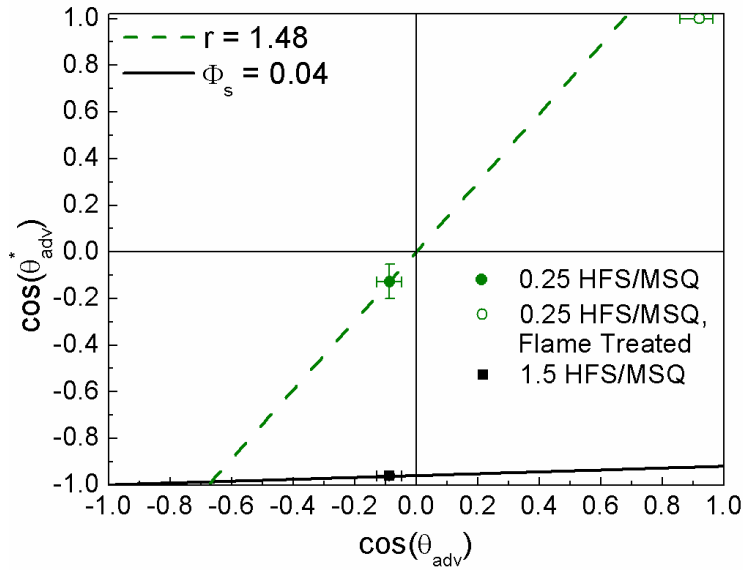
Figure 3. Apparent advancing contact angle θ_{adv}^* for spray cast, HFS filler-containing coatings vs. θ_{adv} for spin-coated MSQ (plotted in terms of their cosines). Coatings contain different concentrations of HFS, as indicated in the legend. Unfilled data points indicate flame-treated coatings. Plotted lines are for the two wetting theories; the dashed line is for Wenzel (Eq. 5 with $r = 1.48$),while the solid line is for Cassie-Baxter (Eq. 4 with $\Phi_s = 0.04$).
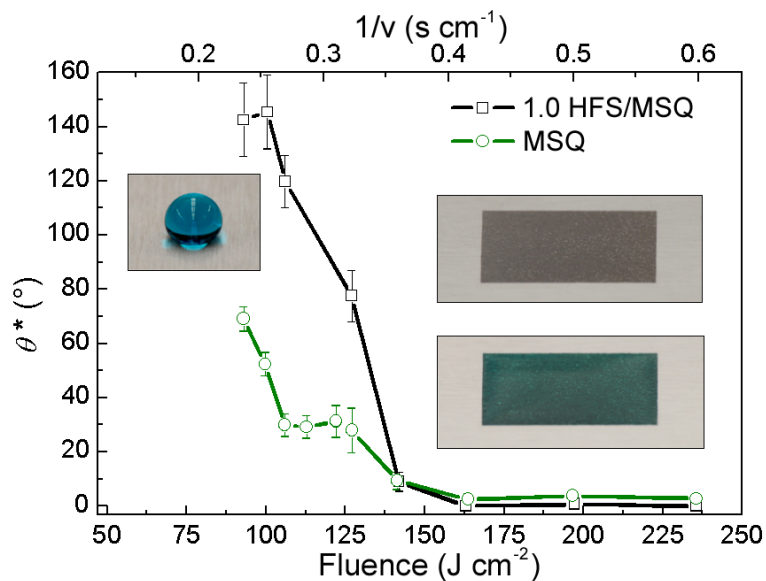
Figure 4. Sessile contact angle (θ^*) vs. laser fluence of the coating (bottom axis) and laser translation speed (top axis; laser irradiance was held constant at $I \approx 0.20$ MW cm^{-2}). Inset images show: (top left) a blue-dyed water droplet on a superhydrophobic coating (1.0 HFS/MSQ mass ratio) prior to laser treatment, (top right) a dry rectangular area of the coating patterned by the laser, and (bottom right) same treated area as above, but fully wetted by a blue-dyed water droplet. The area outside the rectangle is untreated (i.e., remains superhydrophobic), thus remaining dry. All further laser processing was done with a laser translation speed of 2 cm s^{-1}.
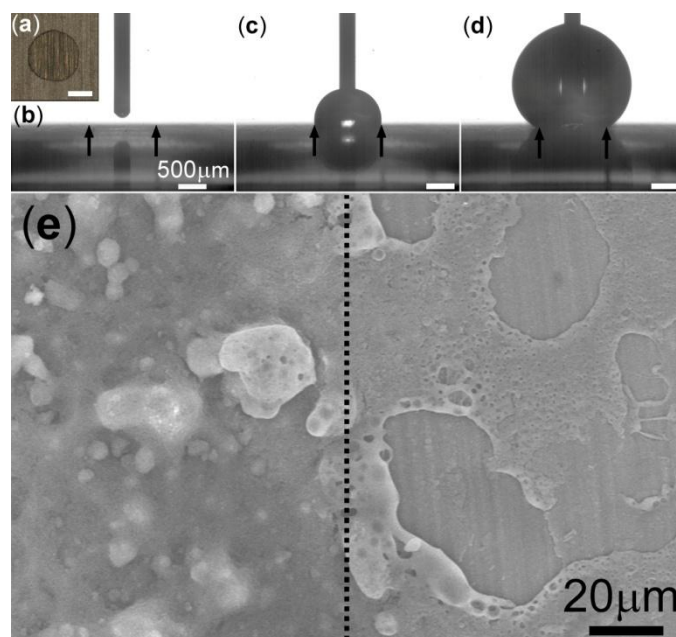
Figure 5. A sequence of images showing an advancing water contact angle measurement at the transition between a superhydrophilic (laser patterned) and the surrounding superhydrophobic area. Inset in (a) shows the laser patterned, hydrophilic, circular spot on the superhydrophobic coating (1.5 HFS/MSQ mass ratio) prior to water droplet deposition (scale bar is 500μm). The scale bars in (c) and (d) are 500 μm. Arrows in (b)-(d) mark the outer extent of the patterned area. Part of the needle in (d) is obscured by the liquid. (e) is a SEM micrograph depicting the transition area with a vertical dashed line separating the hydrophobic (left) from the hydrophilic area (right).
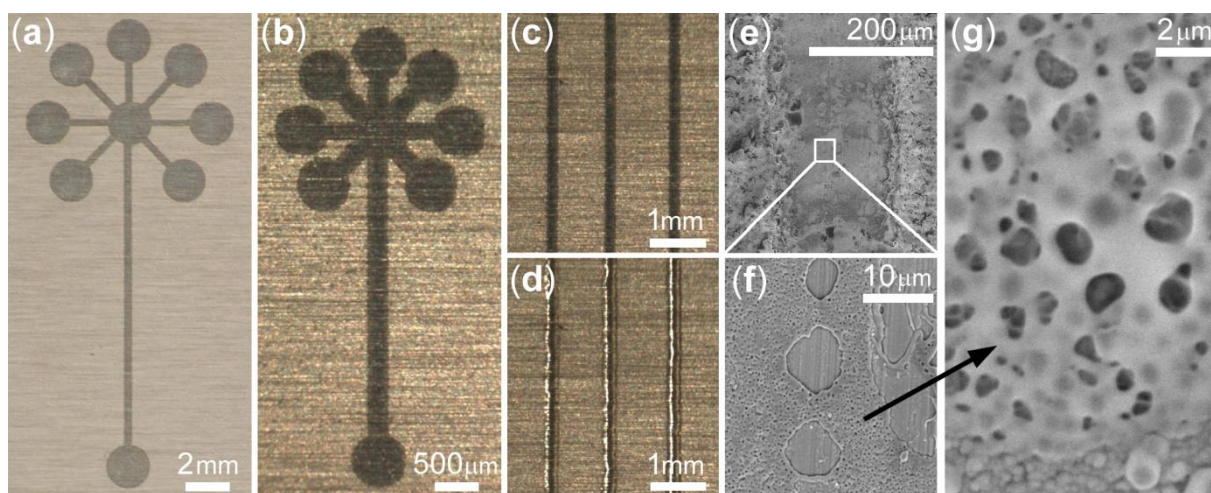
Figure 6. (a) Photographic and (b) optical microscope images of superhydrophilic patterns (dark) on a superhydrophobic MSQ-HFS coating; (c) Hydrophilic, laser patterned lines (dark), and (d) surface-tension-confined channel showing wetting of the lines in (c) by water through capillary action. (e)-(f) SEM images of a STC channel with increasing magnification; (g) SEM image of a laser patterned area revealing porosity. For 0.18 mm-wide STC channels, the water propagation velocity was measured to be 2.5 mm s^{-1}.
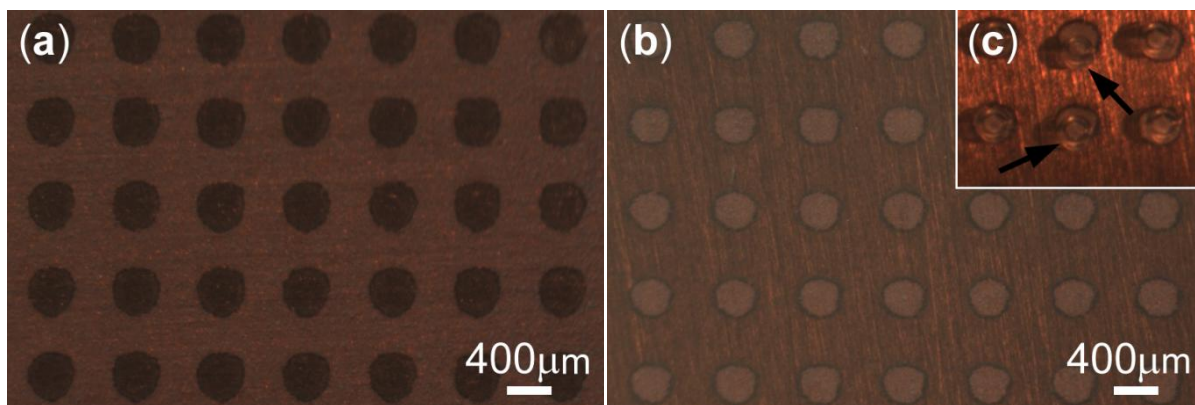
Figure 7. Superhydrophobic MSQ-HFS coating deposited onto copper substrates and laser-processed to create hydrophilic patterns. (a) Superhydrophophilic spots on superhydrophobic background; (b) Superhydrophophobic spots on superhydrophilic background; (c) Pattern from (b) placed in a water bath and subjected to heating; the hydrophobic islands act as preferred gas nucleation sites—arrows indicate vapor bubbles that grow gradually and detach before this cycle repeats itself over and over.
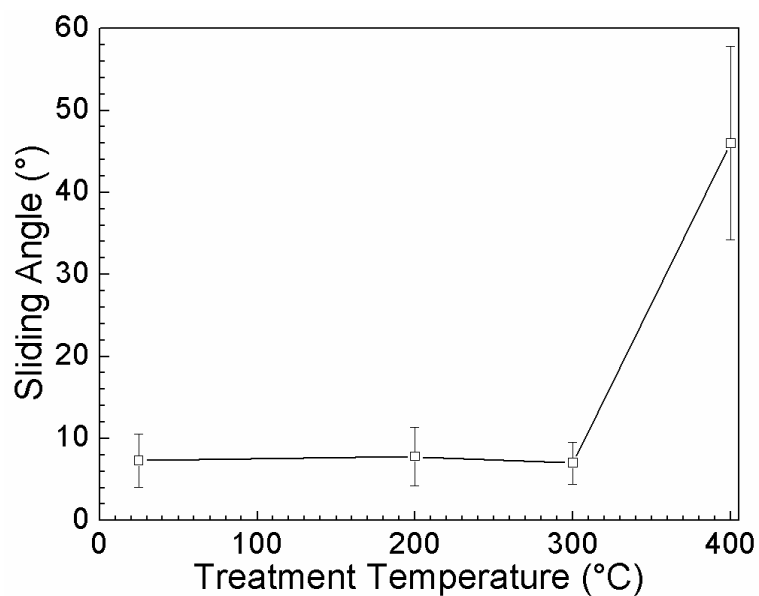
Figure 8. Water droplet sliding angle vs. treatment temperature of a superhydrophobic coating (1.5 HFS/MSQ mass ratio). Coatings were treated for 1 hr on a hot plate in open air. At 500°C treatment temperature, the water droplet ceased to slide, indicating full-loss of the superhydrophobic property of the coating.
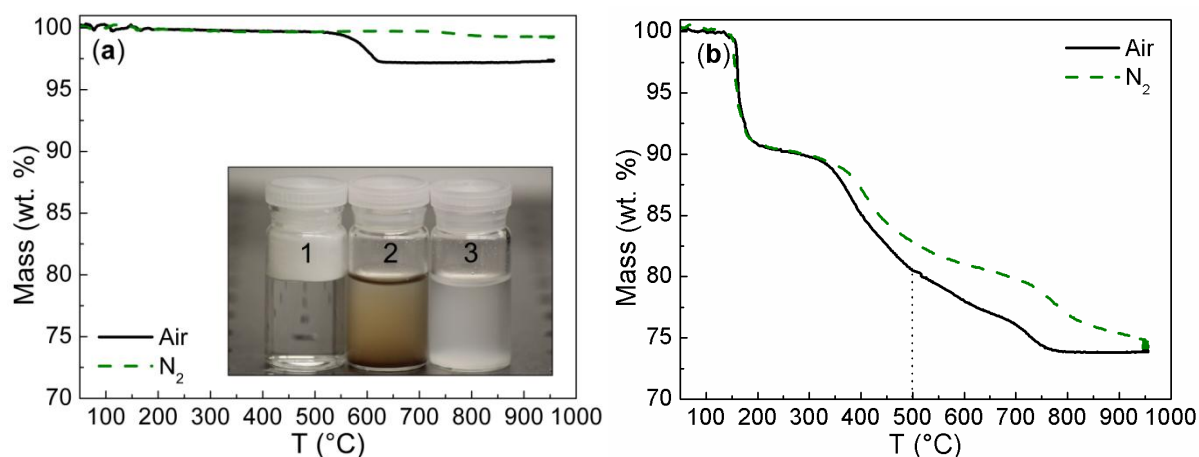
Figure 9. TGA plot (mass vs. T) for (a) HFS, and (b) MSQ under different gas atmospheres (nitrogen, air). The inset in (a) shows three 15 mL glass vials containing 10 g of water and 0.07 g HFS. The HFS contained in vial 1 was not subjected to prior TGA treatment, while the HFS in vials 2 and 3 was. For the HFS in vial 2, TGA was performed under nitrogen conditions. For vial 3 it was run under artificial air conditions. In (b), the dotted (...) drop-down line denotes the thermal treatment temperature (1 hr, open air, hot plate) for a superhydrophobic coating (1.5 HFS/MSQ mass ratio) above which total loss of droplet sliding behavior was observed (see Fig. 8). This temperature marked the beginning of the wettability transition.

Table 1. Composition of dispersions used to make MSQ-HFS coatings

Ingredient	Concentration [wt.%]
20 wt.% MSQ in alcohol	16.7
hydrophobic fumed silica	0.0-8.3
isopropanol	83.3-75.0 (balance)

Table of contents entry

Spray deposition (1) of large-area superhydrophobic coatings (2), and subsequent localized thermal treatment (3) via laser resulted in fabrication of superhydrophilic/superhydrophobic binary patterned areas (4). Using a CO_2 laser, patterned wettability feature sizes of ~100 microns were demonstrated. Such binary patterns are suitable for enhanced heat transfer applications as well as surface tension confined microchannels (i.e., lab on chip).
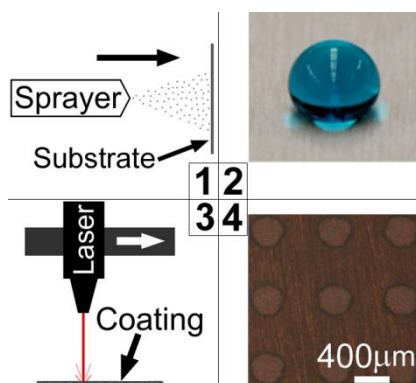
Supporting Information

The photographs shown in **Fig. S1** show the heat-induced change in wettability from superhydrophobic to superhydrophilic. Figure S1a shows three droplets beaded on a superhydrophobic MSQ-HFS coating applied on an aluminum plate. Figure S1b shows the flame treatment using a propane torch; open-air exposure lasted only a few seconds. The flame was operated in the premixed mode, thus assuring the absence of carbonaceous soot (as also affirmed by the blue color of the flame). After flame treatment, the MSQ-HFS coating became superhydrophilic, as shown in Fig. S1c, d and e.

In the case of a semi-infinite solid medium heated on a spot, the corresponding rise in surface temperature (ΔT) can be estimated using the following expression

$$\Delta T(t) = \frac{(1-R)I}{K}\left(\frac{\delta}{\sqrt{\pi}} - \frac{1}{\alpha}\left(1 - e^{(\alpha\delta/2)^2}\text{erfc}(\alpha\delta/2)\right)\right) \tag{S1}$$

Where R is the surface reflection coefficient, I the irradiance (uniform surface source), K the thermal conductivity, δ the diffusion length ($\delta = 2\sqrt{\kappa t}$; with κ being the thermal diffusivity and t the time), and α the absorption coefficient.[1, 2] With $R = 0.05$, $K = 0.01\,\text{W}$ $\text{cm}^{-1}\,\text{K}^{-1}$, $\kappa = 6.0\text{x}10^{-3}\,\text{cm}^2\,\text{s}^{-1}$, $\alpha = 10^3\,\text{cm}^{-1}$ for glass,[2] and $I \approx 0.2\,\text{MW}\,\text{cm}^{-2}$, **Eq. S1** predicts that $\Delta T \sim 2{,}000$ K after only $t = 0.022$ ms, a temperature that is comparable with the propane flame temperature.

Figure S4a-c, Peak 1 and Peak 2 correspond to Si-R and Si-O bonding, respectively. After thermal treatment, an increase in Peak 2 is observed with a corresponding decrease in Peak 1, which can be interpreted as an increase in Si-O bonding with a decrease in hydrophobic groups, i.e., increased hydrophilicity. **d-f**, Peak 1 corresponds to Si-O bonding, and its

concentration increases from **d** to **e** and **f**, suggesting increased hydrophilicity of the coating.

g-i, Peak 1 corresponds to adventitious carbon and/or simple C-H / C-C bonds. Its reduction

from **g** to **h** and **i** is indicative of suspected cleavage of methyl groups, and increased

hydrophilicity.

Figure S6(a)-(b) presents a sequence of SEM micrographs with increasing magnification

from a to b of a spray deposited MSQ-HFS coating (1.0 HFS/MSQ mass ratio) after flame

treatment. This coating displays the property of superhydrophilicity. Note how the

morphology of this coating has relatively little morphological difference as compared with the

untreated version of this coating (see Fig. 1).

Supplementary References

1.   M. von Allmen, *Laser-Beam Interactions with Materials*, Spinger-Verlag, Berlin, 1987.
2.   G. Allcock, P. E. Dyer, G. Elliner and H. V. Snelling, *Journal of Applied Physics*, 1995, **78**, 7295-7303.
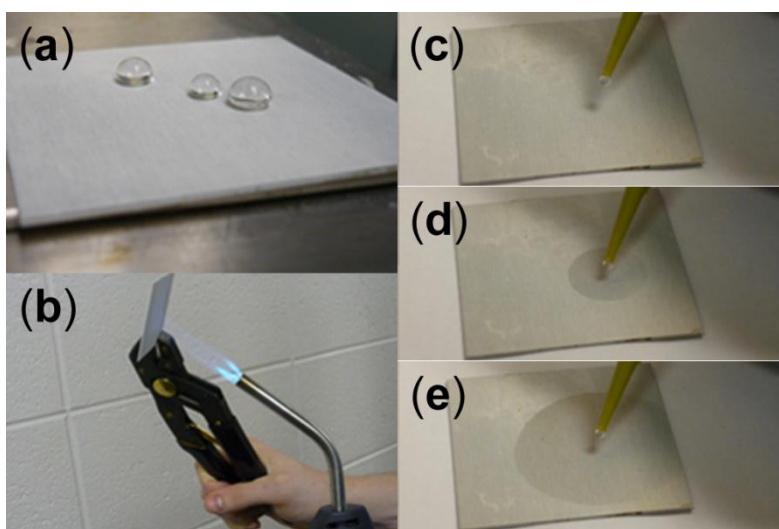
Figure S1. (a) Photograph of beaded water droplets on a MSQ-HFS film applied on an aliminum plate. (b) Flame treatment of the coating shown in (a) using a propane torch for a few seconds from a distance of 5-10 cm. (c) Photograph of the flame-treated coating just before depositing a water droplet (> 10 µL). (d) Completely wetting droplet spreading on the flame-treated coating. (e) Completely wetting droplet at its final fully-spread state.
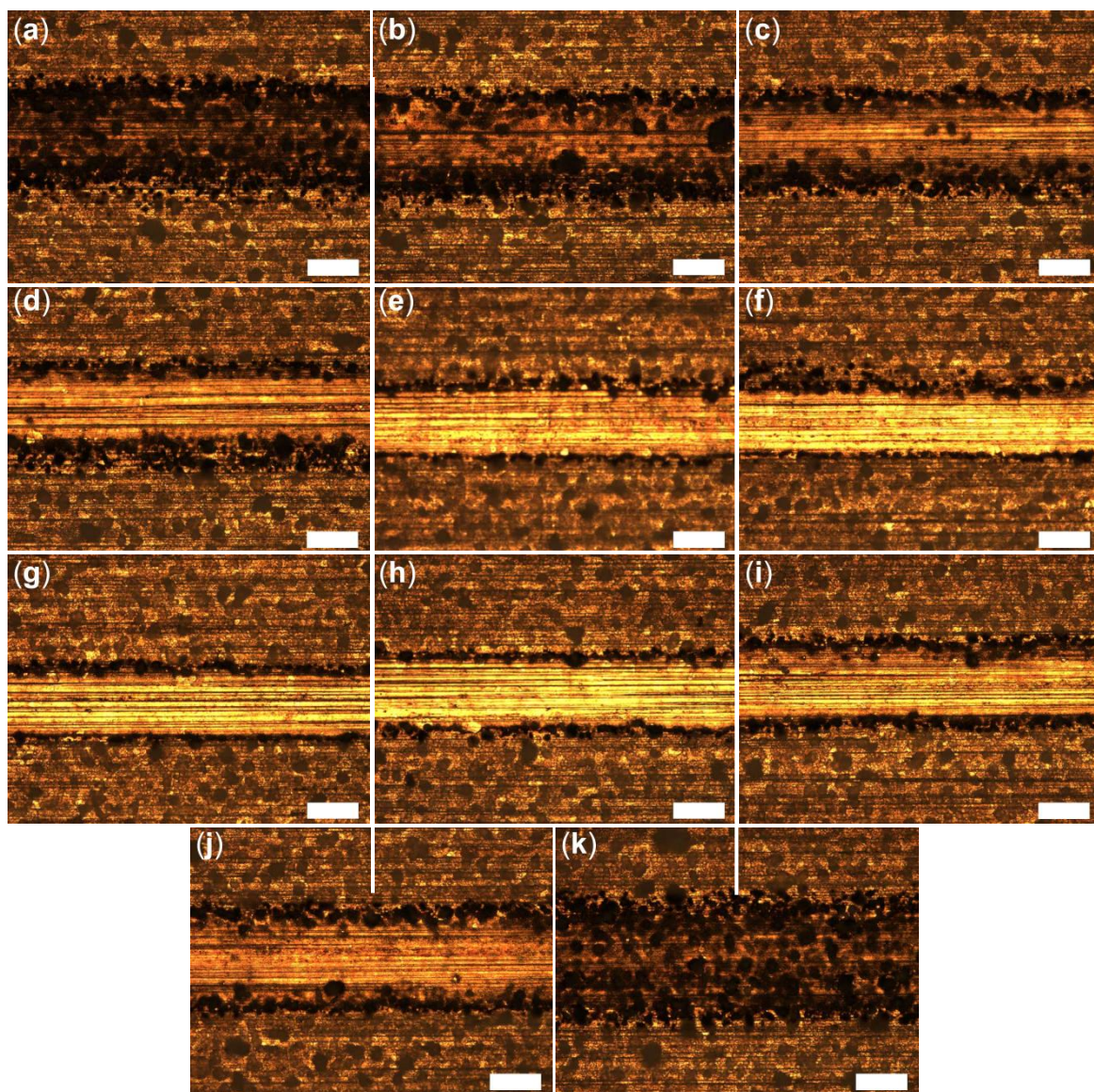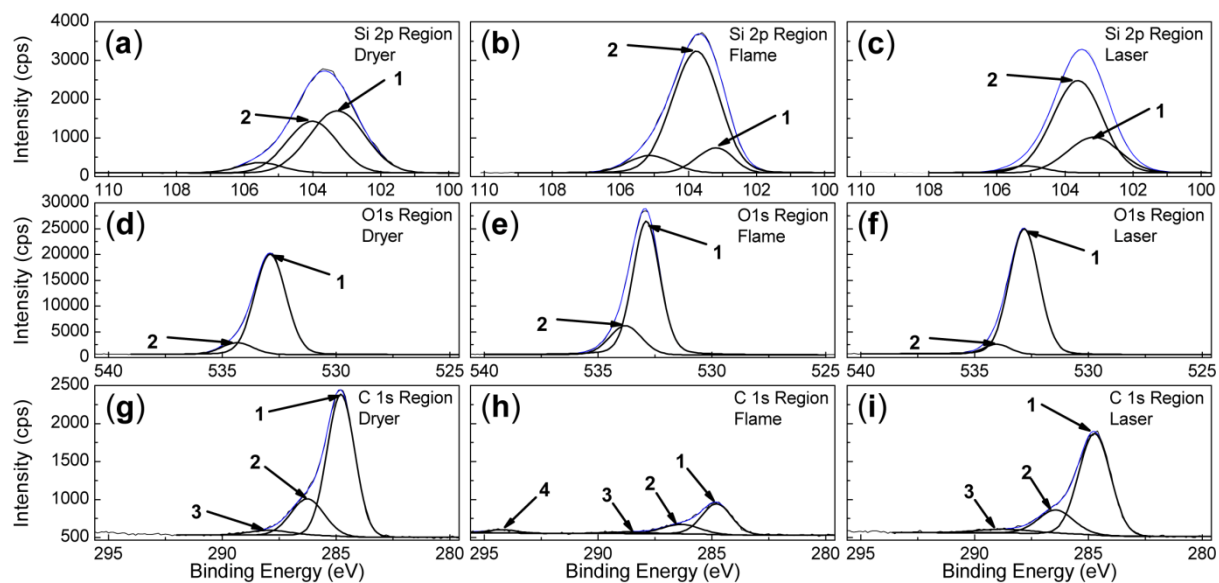
Figure S2. Superhydrophobic MSQ-HFS coatings patterned with a single pass of a CO_2 laser beam at a fixed power (1.0 W) and speed (2.0 cm s^{-1}) with a constant focal length and variable distance between the lens and the substrate. The inset scale bars are 100 μm. The distance between the laser and the substrate is decreasing from (a) to (k) (i.e., (a) has the largest distance between the lens and substrate; (k) has the smallest distance between the lens and substrate). The optimum range is between (e)-(h) with the minimum line width in (g) being 109±6 μm. Inset scale bars in the images are all 100 μm.
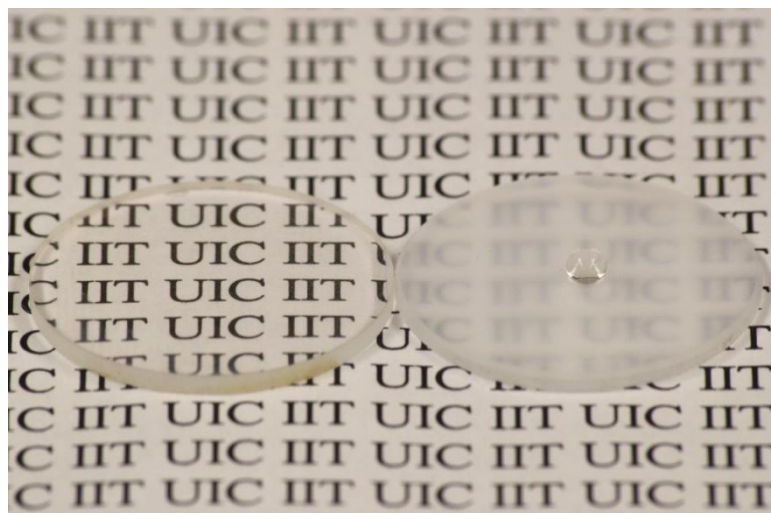
Figure S3. Superhydrophobic MSQ-HFS film deposited onto two quartz substrates (2.54 cm dia.) before (right) and after (left) laser processing, which induces hydrophilicity and increases transparency. A water droplet has been deposited on each surface, but is visible as a bead only on the superhydrophobic disk (right). The droplet on the superhydrophilic disk (left) has fully spread, thus becoming indistinguishable

Figure S4. XPS data of untreated (superhydrophobic) and heat-treated (superhydrophilic) MSQ-HFS coatings. (a)-(c) Si 2p region; (d)-(f) O 1s region; (g)-(i) C 1s region. Figures in the left column represent untreated state, while figures in the middle and right columns are the corresponding thermally treated states. Thermal treatment was performed by either a flame ((b), (e) and (h)) or CO_2 laser ((c), (f) and (i)). For a given region, each peak is designated by a number.

(**a**)   (**b**)

(**c**)   (**d**)
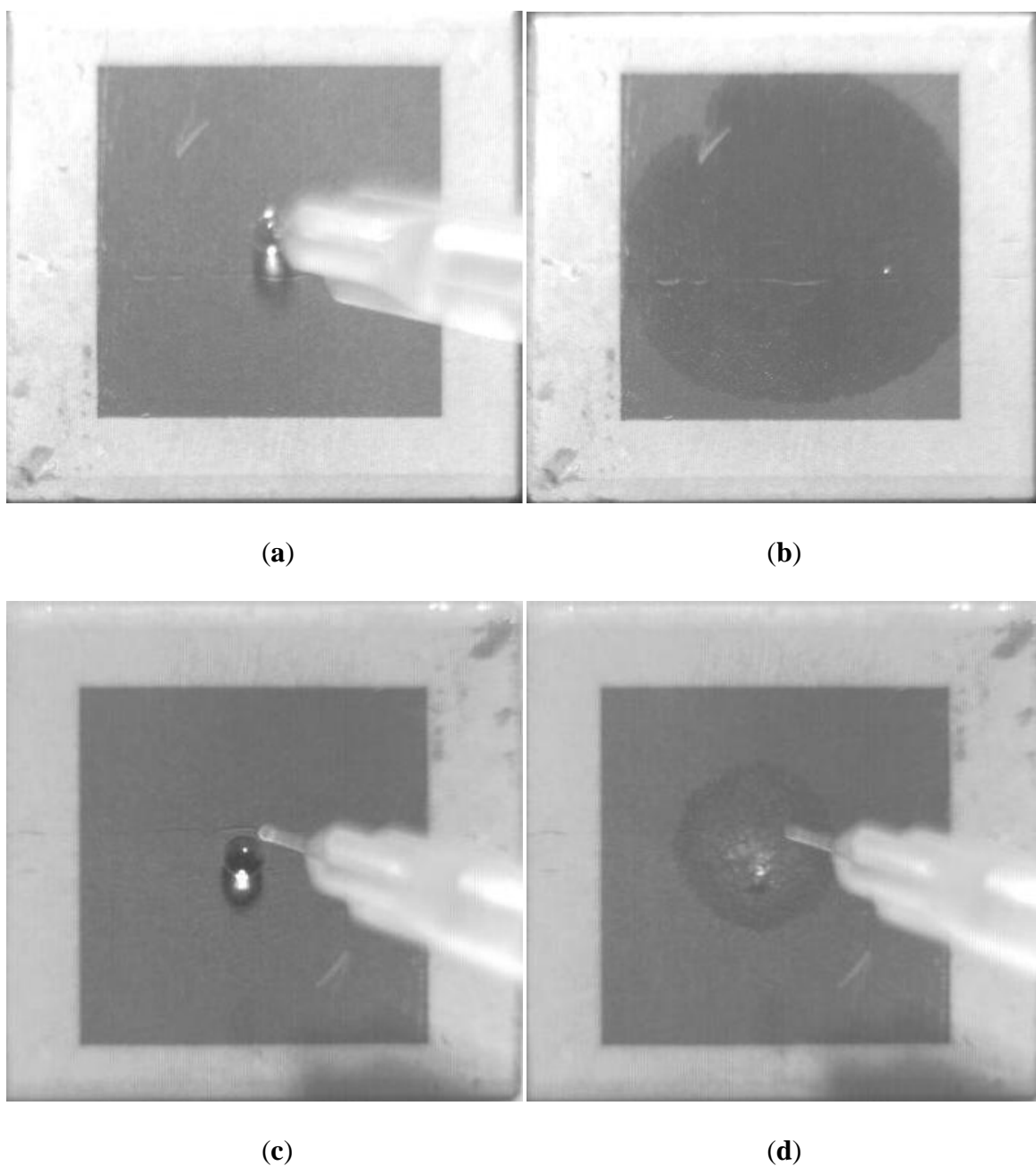
Figure S5 A sequence of images demonstrating the super-wetting behavior of water on laser patterned areas of the MSQ-HFS coating for (a)-(b) room temperature conditions (T=25°C), and (c)-(d) T=138°C. The time difference from (a) to (b) is 1.0 s, and (c) to (d) is 0.4 s. Images were captured with a high speed camera mounted overhead at a frame rate of 250 s^{-1}. The size of the laser patterned areas is 6.4 cm^2; water droplet volumes are < 10 µL.
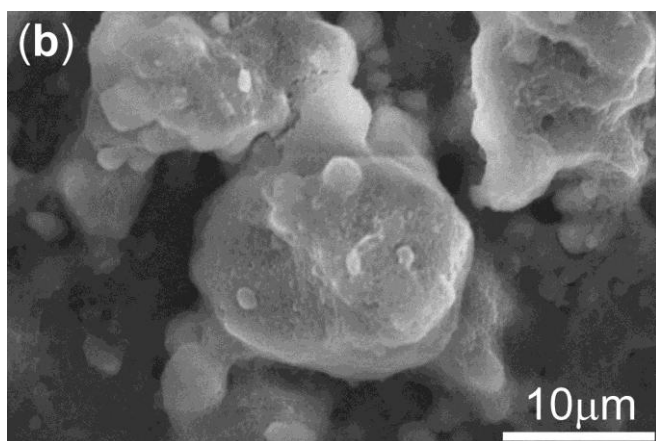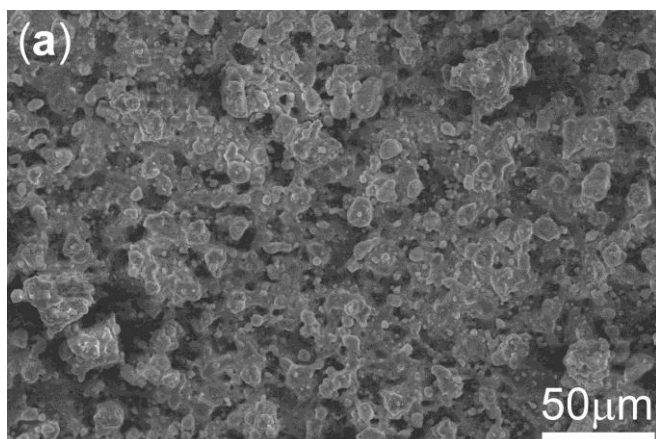
Figure S6 (a)-(b) SEM micrographs of spray deposited MSQ-HFS coatings (1.0 HFS/MSQ mass ratio) with increasing magnification left-to-right after flame treatment (i.e., superhydrophilic coating).